Biomedicine & Pharmacotherapy 183 (2025) 117828

Contents lists available at ScienceDirect

Biomedicine & Pharmacotherapy

journal homepage: www.elsevier.com/locate/biopha

Phosphodiesterase 4D inhibition improves the functional and molecular outcome in a mouse and human model of Charcot Marie Tooth disease 1 A

Melissa Schepers [a,b,1], Tim Vangansewinkel [c,e,1], Karen Libberecht [c,e,1], Hanne Jeurissen [c], Darren Jacobs [a,c], Elisabeth Piccart [a], Robert Prior [d,e,f], Roberta Ricciarelli [g,h], Chiara Brullo [i], Ernesto Fedele [g,j], Olga Bruno [i], Jos Prickaerts [k], Ivo Lambrichts [c], Ludo Van Den Bosch [d,e], Tim Vanmierlo [a,b,*,2], Esther Wolfs [c,**,2]

[a] NIC&R – Neuro-Immune Connection & Repair, BIOMED, Department of Neuroscience, Faculty of Medicine and Life Sciences, Hasselt University, Diepenbeek, Belgium
[b] Department of Psychiatry & Neuropsychology, School for Mental Health and Neuroscience – Division Translational Neuroscience, Maastricht University, Maastricht, the Netherlands
[c] Laboratory for Functional Imaging & Research on Stem Cells, BIOMED, Faculty of Medicine and Life Sciences, Hasselt University, Diepenbeek, Belgium
[d] Department of Neurosciences, Experimental Neurology and Leuven Brain Institute (LBI), KU Leuven – University of Leuven, Leuven, Belgium
[e] VIB, Center for Brain & Disease Research, Laboratory of Neurobiology, Leuven , Belgium
[f] Department of Ophthalmology, Medical Faculty, University of Bonn, Bonn, Germany
[g] IRCCS Ospedale Policlinico San Martino, Genova 16100, Italy
[h] Department of Experimental Medicine, Section of General Pathology, School of Medical and Pharmaceutical Sciences, University of Genoa, Genoa, Italy
[i] Department of Pharmacy, Section of Medicinal Chemistry, School of Medical and Pharmaceutical Sciences, University of Genoa, Genoa, Italy
[j] Department of Pharmacy, Section of Pharmacology and Toxicology, School of Medical and Pharmaceutical Sciences, University of Genoa, Genoa, Italy
[k] Peitho Translational, Maastricht, the Netherlands

ARTICLE INFO

Keywords:
CMT1A
Mouse model
Patient iPSC
PDE4D inhibition
Schwann cells
Remyelination

ABSTRACT

Charcot-Marie-Tooth disease type 1A (CMT1A) is an inherited peripheral neuropathy caused by a duplication of the peripheral myelin protein 22 (PMP22) gene. It is primarily marked by Schwann cell dedifferentiation and demyelination, leading to motor and sensory deficits. Cyclic adenosine monophosphate (cAMP) is crucial for Schwann cell differentiation and maturation. Therefore, increasing cAMP by inhibiting its degraders, phosphodiesterases (PDE), is a potential therapeutic strategy for CMT1A. This study investigated the therapeutic potential of the specific PDE4D inhibitor Gebr32a using the C3-PMP22 mouse model for CMT1A and patient-induced Pluripotent Stem Cell (iPSC)-derived Schwann cells. C3-PMP22 mice, injected subcutaneously with Gebr32a twice a day for 10 weeks, showed significantly increased nerve conduction in sciatic nerves compared to vehicle-injected controls, indicating improved myelination. Additionally, Gebr32a-treated C3-PMP22 mice exhibited improved sensorimotor functions. Grip strength analysis revealed significantly increased strength in all limbs of Gebr32a-treated C3-PMP22 mice. Post-mortem histological and ultrastructural analysis confirmed enhanced myelination in the sciatic nerve of treated mice compared to controls. In primary mouse CMT1A Schwann cells, Gebr32a dose-dependently increased the expression of pro-myelinating genes such as *oct6, Krox20, Mbp, Mpz*, and *Plp*, while downregulating the dedifferentiation marker *c-Jun* and human *PMP22*. Similar effects on gene expression were observed in iPSC-derived Schwann cells from a CMT1A patient, highlighting the clinical relevance of our findings. In conclusion, inhibition of PDE4D with Gebr32a improves the functional and molecular outcomes in mouse and human models of CMT1A, highlighting its potential as a new therapeutic strategy for CMT1A disease management.

* Correspondence to: Maastricht University, Mental Health and Neuroscience Research Institute, Division Translational Neuroscience, Universiteitssingel 50, 6229 ER Maastricht, The Netherlands and also Hasselt University, Biomedical Research Institute, Building C, Agoralaan, Diepenbeek 3590, Belgium.
** Correspondence to: Hasselt University, Biomedical Research Institute, Building C, Agoralaan, Diepenbeek 3590, Belgium.
E-mail addresses: t.vanmierlo@maastrichtuniversity.nl (T. Vanmierlo), esther.wolfs@uhasselt.be (E. Wolfs).
[1] equally contributing first authors
[2] equally contributing last authors

https://doi.org/10.1016/j.biopha.2025.117828
Received 26 September 2024; Received in revised form 3 January 2025; Accepted 9 January 2025
Available online 16 January 2025

1. Introduction

Charcot-Marie-Tooth disease (CMT) is the most common hereditary motor and sensory neuropathy with an estimated prevalence of 1:2500 worldwide [1–4]. CMT is a clinically and genetically heterogeneous disease. Patients typically manifest a slowly progressive, length-dependent degeneration of their peripheral nerves, leading to muscle weakness and atrophy in the feet and legs, which subsequently extends to the hands. The disease progression results in reduced tendon reflexes and slight to moderate distal sensory impairment. Foot deformities, like *pes cavus* and hammer toes, are among the frequently reported manifestations of CMT, with patients regularly exhibiting hearing loss and hip dysplasia. These and other additional symptoms that mark the different CMT subtypes may cause a significant decrease in the quality of life of affected individuals [5].

According to electrophysiological criteria and the specific cell types involved, CMT is broadly categorized into two primary subgroups: CMT1 and CMT2, with intermediate types being recognized. CMT1 is characterized by peripheral nerve demyelination due to damage to the myelinating Schwann cells, which leads to slow nerve conduction velocities (NCVs) (<38 m/s in patients). In contrast, CMT2 is characterized by axonal degeneration and NCVs within the normal (>40–45 m/s) or occasionally in the mildly abnormal range (30–40 m/s). Over 100 genes have been implicated in the pathogenesis of CMT, reflecting its genetic complexity [6].

The myelination of axons by Schwann cells in the peripheral nervous system (PNS) is essential for rapid nerve conduction. In CMT1, mutations cause malformation or deterioration of the myelin sheath, leading to prominent demyelination [6,7]. CMT1A, the most prevalent form, results from an autosomal dominant tandem duplication of the *peripheral myelin protein 22* (*PMP22*) gene, causing overexpression of the PMP22 protein, a key component of compact myelin [8,9]. Despite significant progress in CMT research, effective treatments are currently lacking and tested compounds, such as ascorbic acid, onapristone, and antisense oligonucleotides (ASOs), have shown limited success [10–13].

Addressing the molecular abnormalities driving the Schwann cell phenotype in CMT1A is pivotal for developing new and effective therapeutic strategies. The intracellular second messenger cyclic adenosine monophosphate (cAMP) is instrumental in orchestrating Schwann cell functioning [14]. Physiological modulation of intracellular cAMP levels, and therefore its downstream signaling cascade activation (e.g. MEK-ERK kinase cascade, PI3K-AKT pathway), is crucial for maintaining a proper balance between Schwann cell proliferation and myelination [15]. While low concentrations of cAMP favor Schwann cell proliferation, elevating cAMP levels has been demonstrated to positively regulate Schwann cell differentiation and subsequently myelination [16–19]. Interestingly, a transgenic Sprague-Dawley rat model overexpressing *PMP22*, thereby mimicking CMT1A pathophysiology, displayed a decrease of intracellular cAMP concentrations in CMT1A Schwann cells, highlighting the potential of elevating cAMP levels as a novel therapeutic strategy for correcting Schwann cell functioning in CMT1A [20].

Intracellular cAMP signaling is positively regulated by activation of adenylyl cyclase (AC), while being rapidly terminated by a class of enzymes called phosphodiesterases (PDEs). PDEs can be classified into 11 families (PDE1–11) based on substrate specificity (cAMP and/or cGMP), mechanisms of regulation, kinetic properties, and subcellular distribution [21]. Each family consists of several genes (e.g., PDE4A-4D) and each gene product can have multiple isoforms (e.g., PDE4D1–9), yielding a cell type-specific PDE expression signature [21,22]. In neural tissue, PDE4 is the predominant expressed form and inhibiting its enzymatic activity, thereby increasing intracellular cAMP levels, has been demonstrated to have neuroregenerative effects in the PNS [23–25]. Previously, we have shown that PDE4 inhibition boosts Schwann cell myelination in a 3D regeneration model [26]. However, emetic and gastrointestinal side effects accompanied with non-subtype selective PDE4 inhibitors at their repair-inducing dose significantly decrease their clinical relevance for treating peripheral neuropathies [27]. Interestingly, in the central nervous system (CNS), inhibiting the PDE4D subtype with the small molecule Gebr32a has recently been shown to enhance oligodendrocyte precursor cell differentiation *in vitro* and to induce *in vivo* remyelination at a non-emetic dose, indicating a novel and crucial role for PDE4D in orchestrating (re)myelination processes [28]. Hence, we hypothesize that PDE4D inhibition restores Schwann cell functioning by resolving the derangements in CMT1A Schwann cells.

In this study, we aimed to determine the therapeutic potential of the PDE4D inhibitor Gebr32a for CMT1A. We discovered for the first time that Gebr32a-mediated PDE4D inhibition improved both functional and molecular aspects of CMT1A pathology, as observed in C3-PMP22 mice, primary murine Schwann cells, and iPSC-derived Schwann cells from a CMT1A patient. These findings underscore the therapeutic potential of PDE4D inhibition in correcting Schwann cell dysfunction in CMT1A, offering promising prospects for disease management and rendering the study highly relevant.

2. Materials and methods

2.1. Animals and Gebr32a treatment

The C3-PMP22 (Tg(PMP22)C3) mouse model was obtained from the Academisch Medisch Centrum (University of Amsterdam, The Netherlands) and maintained on a C57BL6/J genetic background [29]. Heterozygous C3 animals were crossbred with wildtype (WT) mice as previously described [29–31], resulting in either heterozygous or WT offspring. Genotyping of the mice was performed as previously described [30].

Mice were kept in filter top cages in a controlled environment with a room temperature between 20 and 21°C, humidity levels between 50 % and 60 %, *ad libitum* access to food and water, and a light–dark cycle of 12 h. All experimental animal procedures were approved by the Ethical Committee for Animal Experimentation (ECAE) of Hasselt University and were performed according to the guidelines described in Directive 2010/63/EU on the protection of animals used for scientific purposes (Matrix ID: 202064).

C3-PMP22 animals were divided and randomized into two groups based on their baseline motor function performances. The vehicle-treated group received 0.1 % DMSO (VWR prolab, Pennsylvania, USA) diluted in 2 % Tween 80 (Merck, Darmstadt, Germany) and 0.5 % methylcellulose (Sigma-Aldrich, St. Louis, Missouri, USA). The Gebr32a-treated group received 0.3 mg/kg Gebr32a (University of Genova [32]) dissolved in the same solution as vehicle (concentrations based on previously determined repair inducing dose [28]). Mice received subcutaneous injections twice a day over a period of 10 weeks with an injection volume of 5 μl/g body weight (see treatment scheme Fig. 1A). Two cohorts of different ages were included: the first cohort received the treatment between 15 and 20 weeks of age and comprised male and female littermates (group 1, WT control n = 5; C3-PMP22 vehicle n = 4; C3-PMP22 Gebr32a n = 4), while the second cohort received the treatment between 30 and 35 weeks of age and comprised male littermates (group 2, WT control n = 7; C3-PMP22 vehicle n = 5; C3-PMP22 Gebr32a n = 5).

2.2. Motor phenotyping

All behavioral assessments were performed in a randomized order and scored by an experimenter blinded for the treatment condition.

2.2.1. Beam walk

Motor coordination was analyzed using a 1 m long beam with a width of either 7, 12, or 18 mm. Beams were placed 1 m above the ground with a black end goal box. Mice were allowed to traverse the beam and the time to cross the inner 80 cm of the beam was measured.

For each mouse, 3 successful runs were recorded. The required time to cross the beam successfully was recorded. A successful run was defined as one continuous movement (no stopping or turning around).

2.2.2. Rotarod

An accelerating mouse-sized Rotarod (Ugo Basile, Italy) was used to evaluate voluntary motor function. Four trials were performed using 4 – 40 RPM acceleration over the course of 5 min, with a minimum of 5 min rest between trials. The latency to fall was recorded.

2.2.3. Grip strength tests

Forelimb grip strength was assessed using a grid connected to a

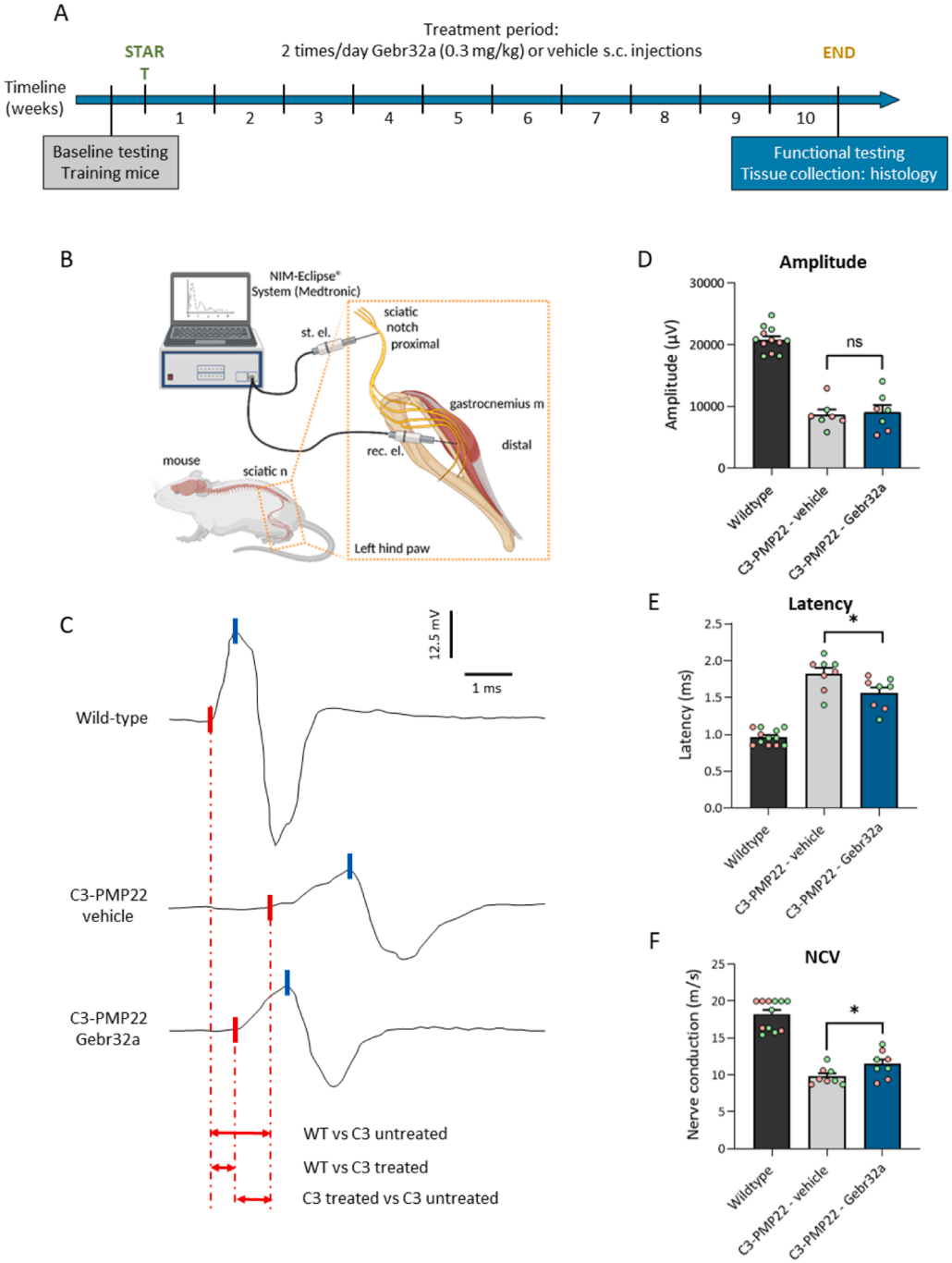

Fig. 1. PDE4D inhibition by Gebr32a significantly improves electrophysiological outcome measurements in the C3-PMP22 mouse model. Wild-type (WT) and C3-PMP22 mice were subcutaneously treated with either the PDE4D inhibitor Gebr32a (0.3 mg/kg) or a vehicle control twice a day for 10 consecutive weeks. **(A)** Timeline illustrating the experimental protocol. (**B**) Illustration of electrophysiological recordings to measure the compound muscle action potentials (CMAP) in the left hind paw at the level of the *m. gastrocnemius* (created with BioRender.com). **(C)** Illustrations representative CMAP traces for WT and C3-PMP22 mice that received no treatment (vehicle) or Gebr32a. The red line indicates the onset of the electrical response and the blue line indicates the maximum amplitude as a measure for the number of axons. **(D-F)** Supramaximal sciatic nerve stimulation reveals no differences in CMAP amplitude (D), while both the latency (E) and nerve conduction speed (F) were significantly improved in C3-PMP22 mice that received Gebr32a. Two different age cohorts were included containing both male and female mice: group 1 (red datapoints) was 10–15 weeks old, and group 2 (green datapoints) was 30–35 weeks old when treatment started. Data are presented as mean ± SEM ($n \geq 7$/group). *$P \leq 0.05$, non-parametric Mann-Whitney test.

LabQuest® Newton meter (Vernier, USA). As the mouse grasped the grid, the pull force was recorded by slowly pulling the animal backwards by the tail until it released its grip. For each animal, 3 grip strength trials were conducted with a minimum of 5 min rest period between each trial, and the average maximum pull force was determined.

2.2.4. Hanging wire

Mice were placed on a cage lid and turned upside down until approximately 10 cm above the cage. The latency to fall was recorded with a maximal cutoff time of 2 min. For each mouse, 3 measurements were recorded with at least 5 min of rest between trials to avoid fatigue.

2.2.5. Grid walk

For the grid walk test, a grid walkway of 1 m long (10 cm width) with a grid size of 2 cm× 2 cm was used. The grid walkway was suspended 1 m above the ground with a black end goal box. A camera was mounted underneath, filming the inner 80 cm of the walkway. Each animal crossed the walkway 3 times. Recordings were analyzed after the run to determine the number of foot slips. Foot slips were defined as a hind paw completely passing through the plane of the wire grid. The average number of foot slips was calculated for each mouse.

2.2.6. Pellet retrieval

The training protocol for evaluating forelimb dominance using the pellet retrieval test was modified from Chen *et al.,* 2014 [20]. Briefly, on the first day, mice were placed individually inside the training chamber after which they were food-restricted. Next, animals gained access to food for 2 h per day for the remainder of the training period. On the second day, mice were placed inside the training chamber with 10 pellets. From the third day onwards, forelimb dominance was determined as previously described [20]. After forelimb dominance was determined for each animal, animals were scored on the final day as described previously [20]. Thirty attempts or 20 min (whichever came first) were recorded and scored (1, success; 2, dropped; 3, fail). From these data, the success rate was calculated for each animal. After initial training, no re-training was needed. After treatment, mice were immediately scored in the same way as on the final day of training.

2.3. Electrophysiology

Compound Muscle Action Potentials (CMAP) of the sciatic nerve were recorded using a NIM-Eclipse® System (Medtronic), as described previously [33]. Briefly, after general anaesthesia, the mouse was placed on a heating pad in the prone position. Stimulating electrodes were subsequently subcutaneously placed at a distance of approximately 2 cm on both sides of the sciatic notch. Next, the gastrocnemius muscle was located, and the recording electrode was placed subcutaneously in alignment. The reference electrode was placed subcutaneously next to the Achilles tendon (30° angle), and the ground electrode was placed subcutaneously on the side of the mouse. Supramaximal stimulation was used to evoke the CMAPs (5–20 mA, up to 60 mA in demyelinating conditions).

2.4. Immunohistochemistry

At the endpoint, sciatic nerves were isolated and 10 μm thick coronal tissue sections were made (Leica, Wetzlar, Germany) for immunohistochemical analysis. Nerve sections were air-dried and heat-induced antigen retrieval was performed using sodium citrate buffer (10 mM, pH 6.0). Sections were blocked with 100 % protein block (DAKO) and incubated overnight with mouse anti-βIII-Tubulin (1:250, T8578 Sigma, Missouri, USA), rat anti-MBP (1:500, MAB386 Millipore, Burlington, Massachusetts), rabbit anti-MPZ (1:500, Abcam, UK) and rabbit anti-KROX20 (1:500, Abcam, UK) at 4°C in a humidified chamber. Following repeated washing steps with PBS, nerve sections were subsequently incubated with Alexa 488- or Alexa 555-conjugated secondary antibodies (1:600, Invitrogen, Thermo Fisher Scientific, Massachusetts, USA). A DAPI (Life Technologies, Thermo Fisher Scientific, Massachusetts, USA) counterstain was performed for cellular nuclei, and sections were mounted. Images were taken with a Zeiss LSM880 or 900 confocal microscope with consistent brightness and contrast settings based on a negative control. Quantitative image analysis was performed blinded on original unmodified photos using the ImageJ open-source software (NIH, Bethesda, MD, USA), and integrated densities were analyzed for βIII Tubulin, MBP, MPZ, and KROX20. To maximize image readability, the contrast and brightness of the representative images were enhanced equally in all groups.

2.5. Transmission electron microscopy

Sciatic nerves were isolated and fixed with 2 % glutaraldehyde. Next, post-fixation was done with 2 %

osmium tetroxide in 0.05 M sodium cacodylate buffer for 1 h at 4°C. Dehydration of the samples was

performed by ascending concentrations of acetone. Then, the dehydrated samples were impregnated overnight in a 1:1 mixture of acetone and araldite epoxy resin. Afterwards, the samples were embedded in araldite epoxy resin at 60°C and ultra-thin sections (60 nm) were cut, perpendicular to the length of the nerve fibers, with a Leica EM UC6 microtome. Sections were transferred to copper grids (Veco B.V) that were coated with 0.7 % formvar. Analysis of the ultra-thin sections was performed with a Jeol JEM-1400 Flash at 80 kV equipped with an Emsis 20NP XAROSA camera system. EM images were taken at 800x magnification with dimensions of 48 × 36 μm^2; from all areas of every fascicle in a distal sciatic nerve cross section for every mouse. Every axon was analysed for each individual mouse to ensure a comprehensive dataset. ImageJ was used to calculate the g-ratio (the ratio of the inner axonal diameter to the total outer diameter), axon diameter, myelin thickness and number of axons per animal. All analyses were conducted by observers blinded to the experimental arm of the study.

2.6. Murine Schwann cell isolation and culturing

Primary mouse Schwann cells were isolated from nerves of C3-PMP22 mice and their WT littermates as previously described [34,35]. Briefly, mice were sacrificed by cervical dislocation, and the sciatic nerves and brachial plexuses were isolated. After removal of the outer connective tissue layer, nerves were mechanically teased and enzymatically digested for 15–18 hours with 0.5 mg/ml collagenase I / 2.5 mg/ml dispase II (Sigma-Aldrich, Missouri, USA) in low proliferation medium consisting of Dulbecco's Modified Eagle Medium (DMEM, Thermo Fisher Scientific, Gibco, USA) at 37°C. The resulting cell suspension was droplet-plated on Poly-L-lysine (4.7×10^{-2} mmol Lysine concentration, Sigma, Missouri, USA)-coated surfaces in high proliferation medium containing DMEM, 10 % Fetal Bovine Serum (FBC, Biowest, Nuaillé, France), 1 % Pen/Strep, 2 μM forskolin (Stem cell Technologies, Canada), 10 ng/ml Nrg-1 type III (Immunotools, Germany) and 5 ng/ml platelet-derived growth factor AA (PDGF-AA, Immunotools, Germany). Cells were cultured at 37°C, 9 % CO_2, and medium was changed every two days. After 15 days, fibroblast contaminations were eliminated from the cultures by performing negative fluorescence-activated cell sorting (FACS) using a FITC-CD90.2 (Thy2) antibody (Biolegend, San Diego, USA). Cells were labeled for 20 min on ice and sorted using the FACSAria™ Fusion device (BD Biosciences, California, USA). Primary Schwann cells were obtained with > 95 % efficiency.

2.7. iPSC cultures

CMT1A patient-derived induced pluripotent stem cells (iPSC) and their isogenic controls (CS67iCMT-n1, isogenic-CS67iCMT, respectively) were provided by the Cedars-Sinai Medical Center's David and

Janet Polak Foundation Stem Cell Core Laboratory [36]. iPSCs were maintained in Essential 8™ (E8) flex medium (Gibco) with penicillin-streptomycin (1000 U/ml) and cultured as described before [37]. Colonies were passaged each week with 0.5 mM EDTA (Invitrogen, Carlsbad, USA) diluted in Dulbecco's phosphate-buffered saline (DPBS; Sigma-Aldrich, Missouri, USA) and plated on Matrigel LDEV-Free, Growth Factor Reduced (GFR) Basement Membrane Matrix (Corning®, New York, USA). Absence of mycoplasma contaminations was routinely checked, and medium was changed three times/week.

2.8. Differentiation of Schwann cell precursors from human iPSCs

The protocol to generate iPSC-SCPs was adapted from Kim *et al.* [38] and recently described by us [39]. Briefly, iPSCs were seeded as a monolayer with 10 µl/ml RevitaCell (Thermo Fisher Scientific, Gibco, Massachusetts, USA) added to the medium. Twenty-four hours later, cells were cultured in neural differentiation medium consisting of 1:1 Neurobasal medium (Thermo Fisher Scientific, Gibco, USA) and DMEM F-12 (Thermo Fisher Scientific, Gibco, Massachusetts, USA), supplemented with 2 mM Glutamax, 0.01 % N2, 20 µM SB 431542, 0.02 % B27, 3 µM Chir 99021, 0.005 % bovine serum albumin (BSA), 0.11 mM β- mercaptoethanol (BME), and 0.01 % Pen/Strep. After 6 days, the medium was supplemented with 50 ng/ml NRG1 type III (Peprotech, #100–03), which is henceforth denoted as iPSC-SCP differentiation medium (SCPDM).

2.9. Differentiation of Schwann cell precursors to Schwann cell-like cells

On day 27, cells were seeded on poly-L-ornithine (PLO, 100 µg/ml) and laminin (5 µg/ml) coated plates in SCPDM. The following day, iPSC-SC induction medium was added (DMEM-F12 supplemented with 100 U/ml Pen/Strep, 40 µM SB 431542, 6 µM Chir 99021, 200 nM Retinoic acid (Sigma-Aldrich, #R2625), 20 ng/ml PDGF-bb (Peprotech, #100–14B), 5 µM FSK (STEMCELL Technologies, #100–0249) and 200 ng/ml NRG1 type III). On day 30, medium was changed to the following composition: DMEM-F12 supplemented with 100 U/ml Pen/Strep, 0.005 % BSA, 20 µM SB 431542, 3 µM Chir 99021, 100 nM Retinoic acid, 10 ng/ml PDGF-bb, 5 µM FSK and 200 ng/ml NRG1 type III. On day 32, medium was switched, and cells were maintained in the final medium: DMEM-F12 supplemented with 100 U/ml Pen/Strep, 0.005 % BSA, 5 µM FSK, and 200 ng/ NRG1 type III. iPSC-SCs were assessed on day 35.

2.10. Quantitative polymerase chain reaction and transcriptomics

Primary mouse Schwann cells and patient iPSC-derived Schwann cells were exposed for 72 hours to three different concentrations of Gebr32a, i.e. 0.3 µM, 1 µM and 3 µM. For transcriptional analysis, mRNA was extracted (Qiagen, Germany), and quality and concentration were assessed using a Nanodrop (Thermo Fisher Scientific, Massachusetts, USA). After synthesis of 5 ng/µl cDNA (Qscript, Quantabio, USA; T-100 Thermal Cycler Bio Rad, USA), a PCR master mix was prepared containing qPCR SYBR Green (Applied Biosystems, Thermo Fisher Scientific, Massachusetts, USA), and primer pairs. Ct values were detected by QuantStudio (Applied Biosystems, Thermo Fisher Scientific, Massachusetts, USA), and fold changes (FC) were normalized against validated housekeeping genes (HKG). An overview of the primers used in this study is listed in Table 1 (mouse primers) and Table 2 (human primers).

2.11. Statistical analysis

For the *in vivo* study, a priori power analyses were conducted using the software G*Power version 3.1.7. Adequate power (1–β-error) was defined as $\geq$ 80 % with an alpha error of 5 %. Since no differences were observed between both animal cohorts in motor function evaluation or electrophysiological measurements, results were pooled to increase statistical power. All statistical analyses were performed using GraphPad Prism 9.4.1 software (GraphPad Software, Inc.) or Microsoft Excel. Data sets were analyzed for normal distribution using the Shapiro-Wilk normality test. Normally distributed data were analysed with an unpaired *t*-test between vehicle and Gebr32a-treated C3-PMP22 mice. Not normally distributed data were statistically analyzed using the non-parametric Mann-Whitney test. For the qPCR data, a two-way ANOVA was performed, followed by a Šidák post hoc test for multiple comparisons (compared to non-treated cells within the same genotype/isogenic line). Data are presented as means ± SEM. Differences were considered statistically significant when $p \leq 0.05$.

Table 1
Mouse primer sequences for the qPCR analysis.

Gene	Forward primer sequence 5'-3'	Reverse primer sequence 5'-3'
hPMP22	CTCTTCACCCTCACCAAG	TGACTTGAGTTTGATTCAGCA
c-Jun	GACCTTCTACGACGATGCCC	GCCAGGTTCAAGGTCATGCT
Sox10	CACGCAGAAAGCTAGCCGAC'	CACTTTCGTTCAGCAACCTCCA
Oct6	CTCCTGGGGTCCTTCTAACT	TTATACACAGATGCGGCTCTC
Krox20	GATCACAGGCAGGAGAGACTGC	TCCGTTCATCTGGTCAAAGGG
Mpz	TCTCAGGTCACGCTCTATGTC	GCCAGCAGTACCGAATCAG
Mbp	CAGCCAGCACCACTCTTGAA	GCCTCTCCTCGGTGAATCTC
P75	CCCTGCCTGGACAGTGTTAC	ACAGGGAGCGGACATACTCT
Plp	TTGTTTGGGAAAATGGCTAGGA	GCAGATGGACAGAAGGTTGGA
Gapdh (HKG)	ACCACAGTCCATGCCATCAC	TCCACCACCCTGTTGCTGTA
ActB (HKG)	GGCTGTATTCCCCTCCATCG	CAGTTGGTAACAATGCCATGT

hPMP22: human peripheral myelin protein 22, SOX10: SRY-BOX transcription factor 10, Krox20/EGR2: early growth response protein 2, Oct6: octamer-binding transcription factor 6 MPZ: Myelin protein zero, MBP: myelin basic protein, P75: neurotrophin receptor for nerve growth factor, PLP: proteolipid protein, GAPDH: Glyceraldehyde-3-phosphate dehydrogenase, ActB: actin B, HKG: housekeeping gene.

Table 2
Human primer sequences for the qPCR analysis.

Gene	Forward primer sequence 5'-3'	Reverse primer sequence 5-'3'
hPMP22	CTCTTCACCCTCACCAAG	TGACTTGAGTTTGATTCAGCA
c-JUN	GGACTCTTTTTGTTCGGTTGCT	CGTCCGGGTGTTTGGTTTT
SOX10	CAAGCTCTGGAGGCTGCTG	TGGTCTTTCTTGTGCTGCAT
KROX20	CCACGTCGGTGACCATCTTT	TTGATCATGCCATCTCCGGC
MPZ	TGCTCTTCTCTTCTTTGGTGCT	AGAAGGAGCAGTGCAGGGT
MBP	GCCGGACCCAAGATGAAAAC	CAGTCCTCTCCCCTTTCCCT
PLP	AAAGGGGGATTTCTACGGGG	CTGGTTTCCCTGCTCACCTT
ACTB (HKG)	GATCATTGCTCCTCCTGAGC	AAAGCCATGCCAATCTCATC
PGK (HKG)	CTGGGCAAGGATGTTCTGTT	GCATCTTTTCCCTTCCCTTC

hPMP22: human peripheral myelin protein 22, SOX10: SRY-BOX transcription factor 10, Krox20: early growth response protein 2, MPZ: Myelin protein zero, MBP: myelin basic protein, PLP: proteolipid protein, ActB: actin B, PGK: phosphoglycerate kinase, HKG: housekeeping gene.

3. Results

3.1. Gebr32a improves the nerve conduction velocity in nerves of C3-PMP22 mice

As a first step, we aimed to determine the therapeutic effect of PDE4D inhibition via Gebr32a in C3-PMP22 mice, a well-established animal model for CMT1A overexpressing 4–5 copies of the human *PMP22* gene in Schwann cells [29–31]. C3-PMP22 animals were divided and randomized into two groups based on their baseline motor function performances, and two different age cohorts were included. One of the treatment groups received Gebr32a and the other group received a vehicle control. WT littermates were included as a control and received only the vehicle treatment. Mice received subcutaneous injections twice a day over a period of 10 weeks as illustrated in Fig. 1A.

To evaluate sciatic nerve function and myelination following Gebr32a treatment, nerve conduction was evaluated using electrophysiological measurements [30]. Upon proximal sciatic nerve stimulation, compound muscle action potentials (CMAPs) were recorded in the distal hind limb muscle tissue (Fig. 1B). Axonal number was assessed by quantifying the amplitude of the measured CMAPs, while the level of myelination was reflected by the latency time of the CMAPs or the nerve conduction speed. Illustrations of representative CMAP traces are shown for WT, C3-PMP22 untreated and treated mice (Fig. 1C). Although no significant differences in CMAP amplitude was detected (Fig. 1D), Gebr32a treatment significantly reduced the latency time of the CMAP signal and also improved the nerve conduction velocity (Fig. 1E, F), indicative of enhanced myelination. Importantly, both age cohorts showed comparable responses after Gebr32a treatment, as illustrated by the coloured datapoints in Fig. 1D, E, and F (group 1: red *vs.* group 2: green, see methods).

3.2. *Gebr32a improves sensorimotor functions and coordination in C3-PMP22 mice*

Next, we performed multiple motor function and coordination tasks to evaluate the therapeutic effect of the PDE4D inhibitor Gebr32a. Motor coordination was assessed using the beam walk test. C3-PMP22 animals took a significantly longer time to pass both a 12 mm and 7 mm wide beam compared to WT animals. However, upon Gebr32a treatment, C3-PMP22 mice were able to pass the 7 mm wide beam walk significantly faster compared to untreated mice (Fig. 2A).

Endurance, motor balance, and evoked voluntary motor movement were assessed using the rotarod. While WT animals could stay significantly longer on the rotarod, C3-PMP22 mice showed a reduced latency to fall. Although not significant (P = 0.06), Gebr32a-mediated PDE4D inhibition showed an increased latency to fall in C3-PMP22 animals (Fig. 2B).

To assess grip strength, mice were subjected to the grip strength and hanging wire tests. While forelimb grip strength is reduced upon CMT1A pathology, Gebr32a significantly increased grip strength in C3-PMP22 mice (Fig. 2C). Additionally, the latency to fall in the hanging wire test was significantly increased upon Gebr32a treatment in C3-PMP22 animals compared to untreated controls (Fig. 2D).

Sensorimotor functions were assessed using the grid walk test. After allowing the animals to transverse a wire grid, the number of hind paw slips through the grid was determined, which demonstrated an impaired sensorimotor function in C3-PMP22 animals. Upon Gebr32a treatment, C3-PMP22 mice displayed a reduced number of foot slips through the wire grid (Fig. 2E).

Finally, forelimb dominance and coordination were evaluated using

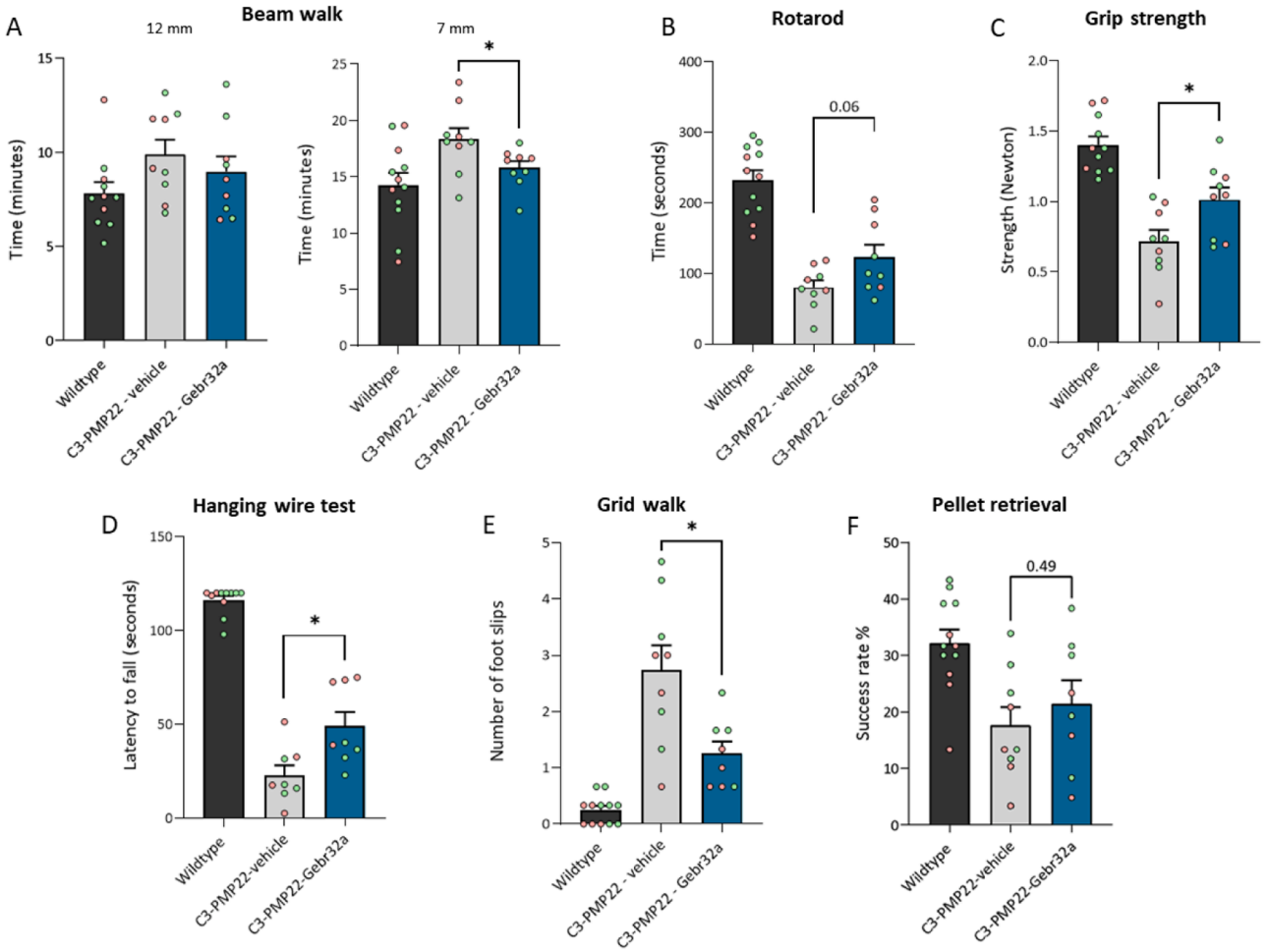

Fig. 2. Gebr32a treatment significantly enhances sensorimotor functions and coordination in C3-PMP22 mice. Sensorimotor functions and coordination were analyzed at the end of the treatment (10 weeks) for WT controls and C3-PMP22 animals treated with the PDE4D inhibitor Gebr32a or a vehicle. Gebr32a treatment results in increased (**A**) motor coordination as assessed using the beam walk test, (**B**) rotarod-evoked motor endurance, (**C-D**) grip strength, and (**E**) sensorimotor function. (**F**) Gebr32a did not alter the pellet retrieval success rate. Data are presented as mean ± SEM (n ≥ 7/group). Two different age cohorts were included containing both male and female mice: group 1 (red datapoints) was 10–15 weeks old, and group 2 (green datapoints) was 30–35 weeks old when treatment started. *$P \leq 0.05$, non-parametric Mann-Whitney test.

the pellet retrieval task. For each animal, 30 reaching attempts were recorded, and the rate of successfully grabbing and feeding the pellet into the mouth was determined. Forelimb coordination was affected in C3-PMP22 mice, as demonstrated by the significantly lower success rate. Yet, Gebr32a treatment could not rescue the pellet retrieval success rate (Fig. 2F). Importantly, both age cohorts showed comparable responses after Gebr32a treatment on the different motor function and coordination tasks, as illustrated by the coloured datapoint in all the graphs of Fig. 2 (group 1: red vs group 2: green).

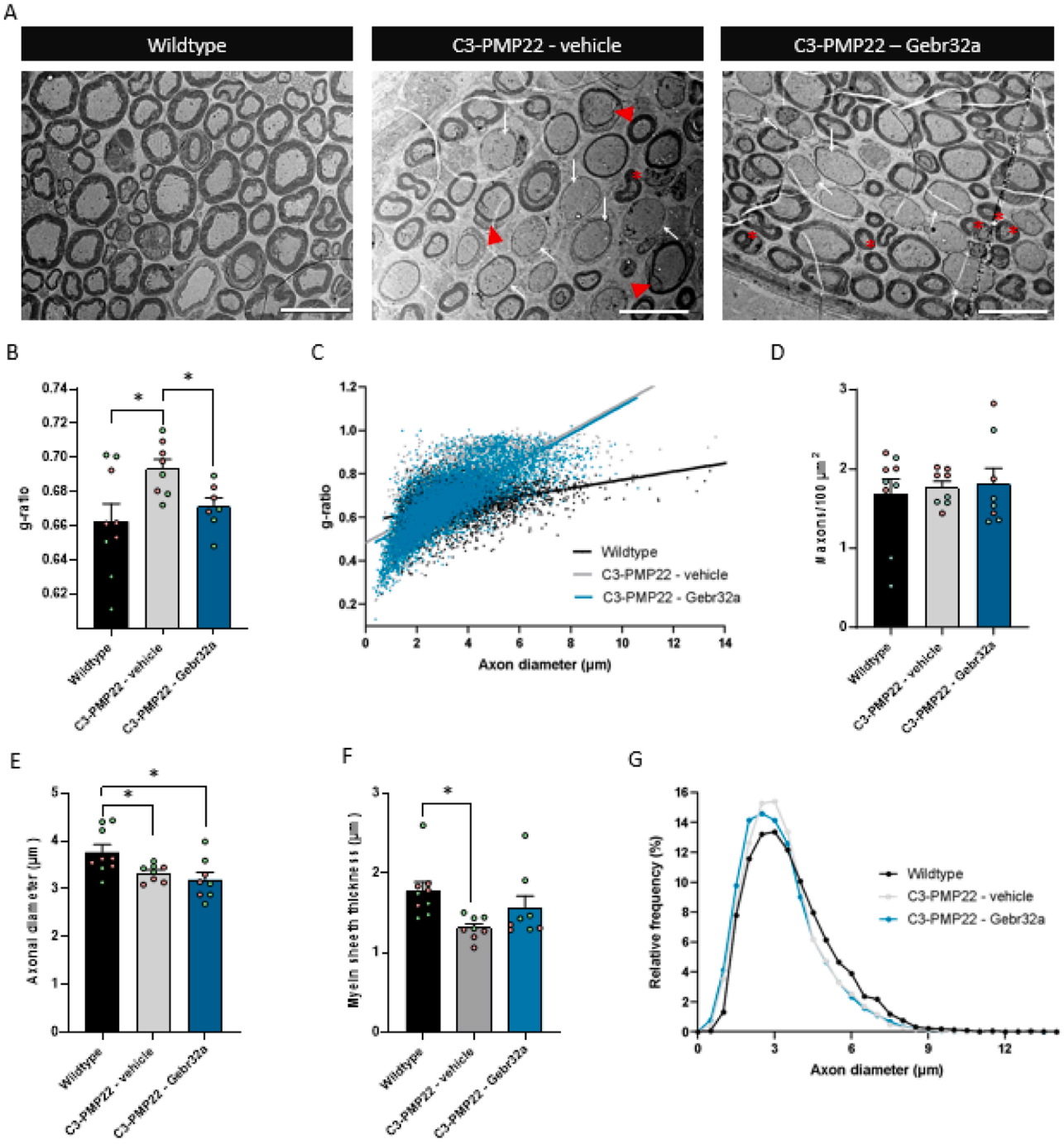

Fig. 3. TEM analysis demonstrates improved myelination at the ultrastructural level in C3-PMP22 mice that received Gebr32a. **(A)** Representative electron microscopy images of distal sciatic nerve cross sections from WT control, C3-PMP22 control and C3-PMP22 Gebr32a-treated groups. Scale bar = 10 µm. Schwann cell dysmyelination is indicated by red arrowheads, hypermyelination by red asterisks, and hypomyelination by white arrows. **(B-C)** Analysis of g-ratios (i.e., ratio inner diameter: outer diameter) indicates lower g-ratios and thereby improved myelination in Gebr32a-treated C3-PMP22 mice compared to untreated controls. **(D-F)** The average number of axons per 100 µm^2 (D), the average myelin sheath thickness (E), and the average axon diameter (F) were quantified and compared between all the groups. Data are presented as mean ± SEM (n ≥ 7/group). No significant differences were revealed by the non-parametric Mann-Whitney test. **(B)** Histogram of the relative frequency distribution of the axon diameters. A simple linear regression, two-tailed statistical test was used to analyze the difference between the cumulative distribution curves of each sample. Two different age cohorts were included containing both male and female mice: group 1 (red datapoints) was 10–15 weeks old, and group 2 (green datapoints) was 30–35 weeks old when treatment started. *$P \leq 0.05$; **$P < 0.01$.

3.3. Post-mortem tissue analysis reveals improved myelination in Gebr32a-treated C3-PMP22 mice

At the end of the treatment, mice were sacrificed, and *post-mortem* tissue analysis was performed on distal sciatic nerve cross-sections. First, electron microscopy was used to explore the effect of Gebr32a treatment on myelination at the ultrastructural level. Representative TEM images are shown of sciatic nerves from WT, C3-PMP22 control, and C3-PMP22 Gebr32a-treated mice (Fig. 3A). Ultrastructurally, we observed signs of dysmyelination, hypermyelination and hypomyelination in nerve tissue of both untreated and treated C3-PMP22 mice, compared to WT littermate controls. Overall myelination was significantly improved, as indicated by significantly reduced g-ratio levels in C3-PMP22 mice that received Gebr32a (Fig. 3B, C). Yet, no significant differences were observed between the groups regarding the average number of axons per area (Fig. 3D) or the average axon diameter (Fig. 3E). However, a non-significant increase in the average myelin sheath thickness in Gebr32a-treated C3-PMP22 mice compared to untreated controls was observed ($P = 0.1314$) (Fig. 3F). A histogram of the relative frequency distribution of axon diameters also showed no differences between the groups (Fig. 3G).

Next, immunohistochemistry was performed to study myelination in nerve cross-sections for βIII tubulin (axonal marker), MBP (myelin marker), KROX20 (Schwann cell differentiation marker), and MPZ (myelin marker). While C3-PMP22 mice showed a lower level of both βIII Tubulin and MBP compared to WT mice, Gebr32a-mediated PDE4D inhibition significantly elevated the presence of both markers (Fig. 4A, B, and C). Similarly, Gebr32a-mediated PDE4D inhibition significantly enhanced the level of both KROX20 and MPZ in the sciatic nerve of C3-PMP22 mice, indicating enhanced Schwann cell differentiation and myelination (Fig. 4D, E, and F). Similar effects on myelination were observed for both age cohorts after Gebr32a treatment.

3.4. Gebr32a dose-dependently stimulates myelin-related gene expression and reduces hPMP22 overexpression in mouse CMT1A Schwann cells

To evaluate the effect of PDE4D inhibition on Schwann cell phenotype and myelin gene expression, primary mouse Schwann cells isolated from either C3-PMP22 mice or WT littermate controls were exposed for 72 hours to different concentrations of Gebr32a (0 μM – 0.3 μM – 1 μM –

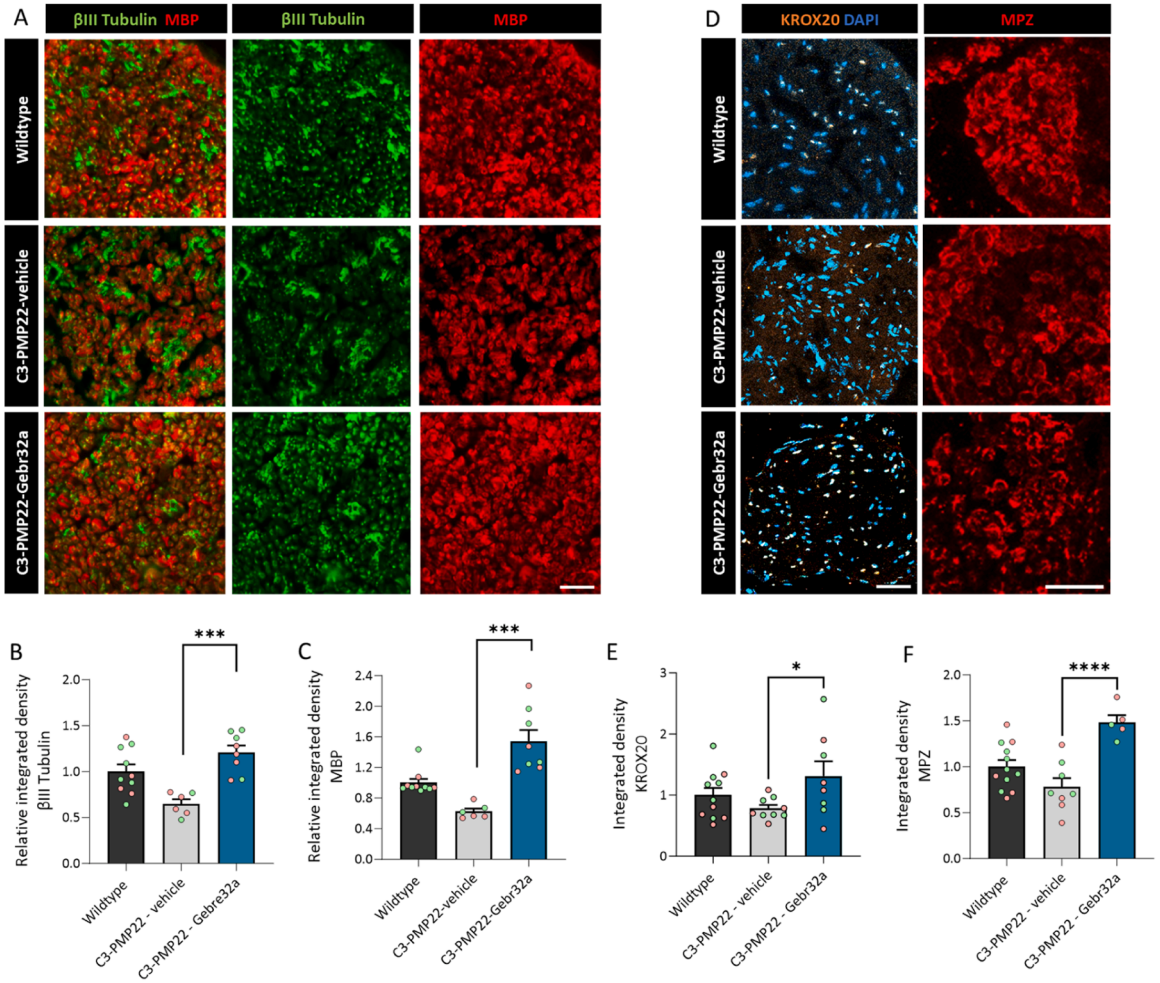

Fig. 4. Gebr32a treatment significantly increases βIII Tubulin and myelin protein expression in the sciatic nerve of C3-PMP22 mice. To measure the expression of axonal and myelin markers, immunohistochemistry was performed on sciatic nerve tissue of WT mice and C3-PMP22 mice that received Gebr32a or no treatment. **(A-C)** Representative images and analysis of the βIII Tubulin (green) and MBP (red). Gebr32a significantly increased βIII Tubulin (B, axonal marker) and MBP (C, myelin protein) protein expression in the sciatic nerve of C3-PMP22 mice compared to control mice. Scale bar = 50 μm. **(D-F)** Representative images of the MPZ (red) and KROX20 (orange). Gebr32a significantly increased MPZ (E, myelin protein) and Krox20 (F, Schwann cell myelination transcription factor) in the sciatic nerve of C3-PMP22 mice. Nuclei are visualized with DAPI (blue). Scale bar = 50 μm. Data are presented as mean ± SEM (n ≥ 6/group). βIII-tubulin, MPZ, and Krox20 were analyzed using a parametric *t*-test, while MBP levels were evaluated using a non-parametric Mann-Whitney test. Two different age cohorts were included containing both male and female mice: group 1 (red datapoints) was 10–15 weeks old, and group 2 (green datapoints) was 30–35 weeks old when treatment started. *$P \leq 0.05$, * **$P \leq 0.001$, * ** *$P \leq 0.0001$. MBP: myelin basic protein; MPZ: myelin protein zero; Krox20/EGR2: early growth response protein 2.

3 μM). Two-way ANOVA analysis highlights only a genotype effect for both *hPMP22* (***$P \leq 0.005$) and *p75* (***$P \leq 0.05$), while significant treatment effects were observed for *hPMP22* (**$P \leq 0.01$), *c-Jun* (*$P \leq 0.05$), *Krox20* (**$P \leq 0.01$), *Sox10* (*$P \leq 0.05$), *p75* (***$P \leq 0.005$), *Plp* (***$P \leq 0.005$), *Mbp* (*$P \leq 0.05$), and *Mpz* (***$P \leq 0.005$). Detailed transcriptional analysis using Šidák multiple comparison analysis indicated that inhibition of PDE4D with Gebr32a significantly reduced *hPMP22* expression at all concentrations (Fig. 5A). Moreover, we observed a significant reduction in *c-Jun* expression (Fig. 5B, i.e., a dedifferentiation marker), and a significant increase in the expression of the pro-myelinating genes *Oct6* (Fig. 5C) and *Krox20* (Fig. 5D) in Gebr32a-treated C3-PMP22 Schwann cells. In addition, *Sox10* (Fig. 5E) and *P75* (Fig. 5F), two Schwann cell lineage markers, show a non-significant and significant increase after Gebr32a treatment in C3-PMP22 Schwann cells, respectively. Moreover, the expression of the mature myelin markers *Mbp*, *Plp,* and *Mpz* were significantly increased after Gebr32 treatment in C3-PMP22 Schwann cells (Fig. 5G-I).

3.5. *Gebr32a promotes myelin-related gene expression and reduces PMP22 overexpression in a dose-dependent manner in CMT1A patient iPSC-derived Schwann cells*

We explored the effect of PDE4D inhibition in a human context, using CMT1A patient iPSC lines, CS67i-CMT-n1, and its isogenic control, isogenic-CS67i-CMT (further referred to as “CMT1A” and “isogenic”

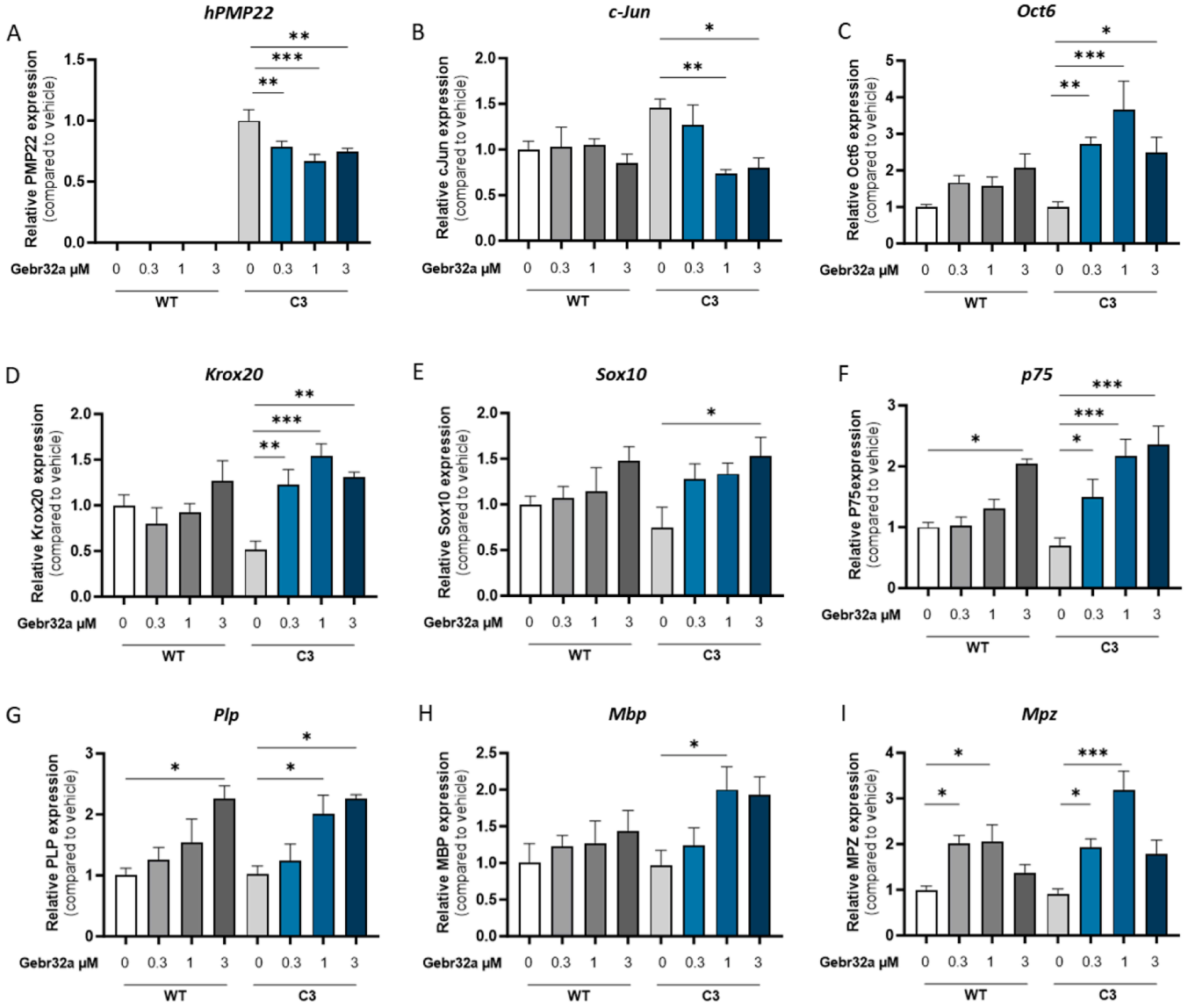

Fig. 5. Gebr32a stimulates the expression of pro-myelinating genes in primary mouse CMT1A Schwann cells. Primary mouse Schwann cells obtained from C3-PMP22 mice and WT littermates were exposed to different concentrations of Gebr32a (0.3, 1 and 3 μM) and gene expression levels were determined. **(A, B)** Gebr32a dose-dependently decreased the mRNA levels of *hPMP22* and *c*-Jun in Schwann cells from C3-PMP22 mice, compared to untreated controls. While *hPMP22* was significantly reduced at all Gebr32a concentrations, c-Jun levels were significantly reduced starting at 1 μM of Gebr32a stimulation. **(C, D)** In addition, the expression of pro-myelinating genes *Oct6* and *Krox20* was significantly and dose-dependently increased after Gebr32a treatment. **(E)** Moreover, a significant increase in *Sox10* expression was observed after 3 μM of Gebr32a treatment. **(F)** Significantly increased *P75* gene expression in a dose-dependent manner in C3-PMP22 Schwann cells after Gebr32 stimulation. **(G-I)** Expression of myelin genes *Mbp*, *Plp,* and *Mpz* was significantly upregulated in Gebr32a-treated C3-PMP22 Schwann cells. Data were normalized against WT Schwann cells that received vehicle treatment. Statistical analysis was performed using two-way ANOVA with Šidák post hoc test for multiple comparisons. n = 3 individual experiments with each 2–3 technical replicates. *$P \leq 0.05$, * *$P \leq 0.01$, * **$P \leq 0.005$. MPZ: myelin protein zero, MBP: myelin basic protein, SOX10: SRY-BOX transcription factor 10, PLP: proteolipid protein, P75: neurotrophin receptor for nerve growth factor, Krox20: early growth response protein 2.

lines, respectively). First, these iPSC lines were differentiated towards immature Schwann cells. Two-way ANOVA analysis demonstrates a genotype-dependent alteration in the expression of *hPMP22* (*$P \leq 0.05$), *c-Jun* (***$P \leq 0.005$), *Krox20* (**$P \leq 0.01$) and *MPZ* (*$P \leq 0.05$). Furthermore, a treatment effect was observed for all genes tested (***$P \leq 0.005$). Šidák multiple comparison analysis illustrates that, after 72 hours of Gebr32a treatment (0 μM – 0.3 μM – 1 μM – 3 μM), a reduced expression of *hPMP22* and *c-Jun* was observed (Fig. 6A, B). Moreover, key pro-myelinating genes, such as *KROX20* and *SOX10* show significantly higher expression levels in Gebr32a-treated CMT1A Schwann cells (Fig. 6C, D). Importantly, the expression levels of myelin genes *MPZ* (Fig. 6E), *MBP* (Fig. 6F), and *PLP* (Fig. 6G) were significantly higher in Gebr32a-treated CMT1A Schwann cells compared to untreated cells.

4. Discussion

The autosomal duplication of the *PMP22* gene in CMT1A patients results in a demyelinating peripheral neuropathy with clinical symptoms arising within the first two decades of life. The lifelong chronic demyelination leaves axons vulnerable, ultimately leading to secondary neuroaxonal pathologies and neurodegeneration. However, no effective treatment exists that restores the CMT1A-induced Schwann cell malformations and, thereby, peripheral myelination. Here, we demonstrated that the PDE4D inhibitor Gebr32a significantly improved the functional and molecular outcome in the C3-PMP22 animal model for CMT1A and in iPSC-derived Schwann cells from a CMT1A patient. For the first time, these data demonstrate the potential of PDE4D inhibition in restoring CMT1A-induced Schwann cell dysfunctions, thereby highlighting its therapeutic potential in CMT1A pathology.

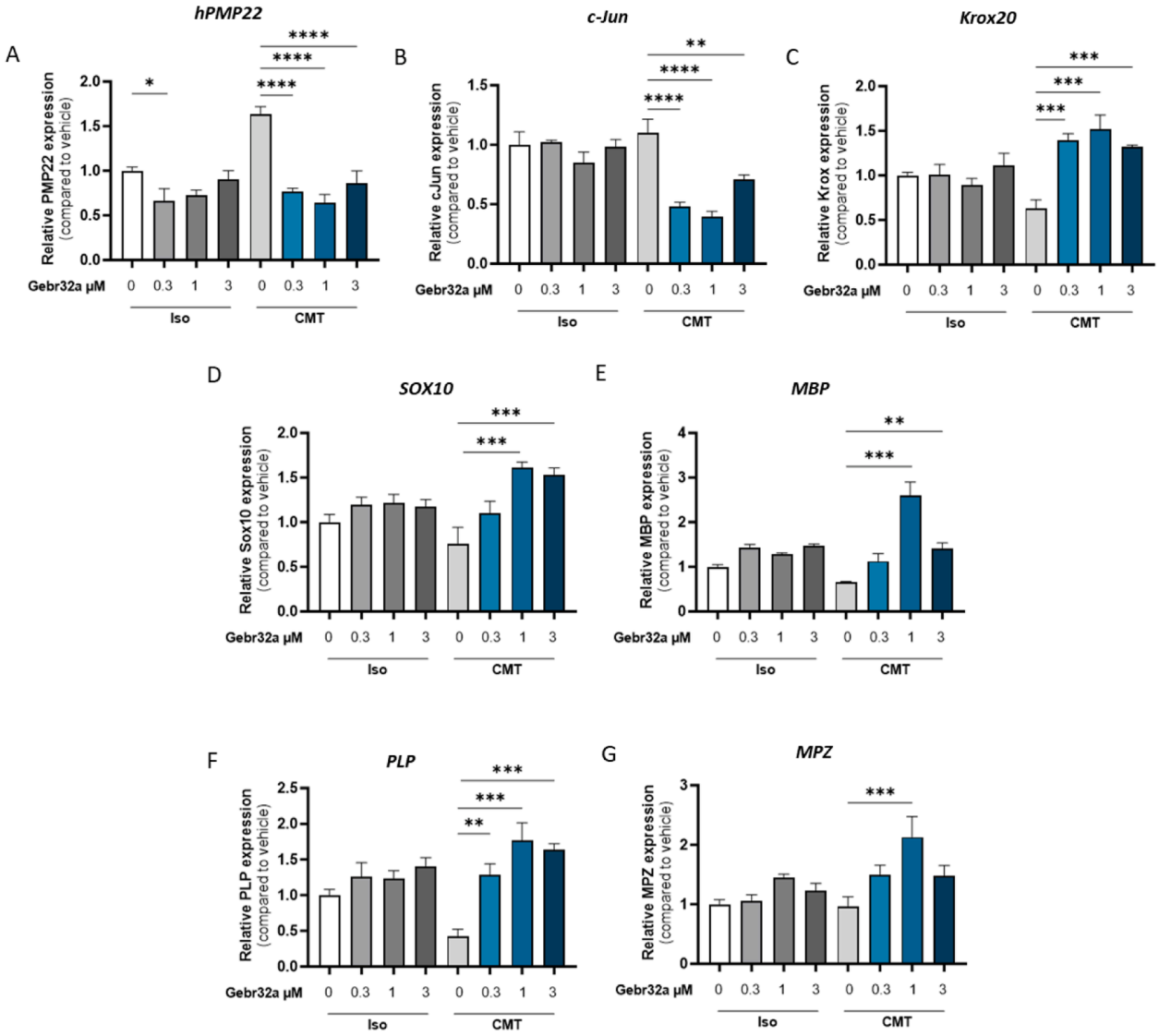

Fig. 6. Gebr32a stimulates the expression of pro-myelinating genes in a CMT1A patient iPSC-derived Schwann cell model. CMT1A patient iPSC-derived Schwann cells and isogenic controls were treated with different concentrations of Gebr32a (0.3, 1 and 3 μM) and gene expression was assessed. **(A, B)** The expression of both *hPMP22* (A) and *c-Jun* (B) was downregulated in CMT1A after Gebr32a exposure. **(C, D)** In contrast, the expression levels of the transcriptional regulators *Krox20* (C) and *SOX10* (D) were significantly upregulated in a dose-dependent manner in Gebr32a-treated CMT1A Schwann cells. **(E-G)** In addition, the expression of the myelin genes *MBP*, *PLP,* and *MPZ* was significantly upregulated following Gebr32a treatment. Data were normalized against untreated isogenic control cells. Statistical analysis was performed using a two-way ANOVA with Šidák post hoc test for multiple comparisons (compared to non-treated group of the same isogenic condition). n = 4 individual experiments with 1 technical replicate. *$P \leq 0.05$, * *$P \leq 0.01$, * **$P \leq 0.005$, * ** *$P \leq 0.001$) MPZ: myelin protein zero, MBP: myelin basic protein, SOX10: SRY-BOX transcription factor 10, PLP: proteolipid protein, P75: neurotrophin receptor for nerve growth factor, Krox20: early growth response protein 2.

Developing (re)myelination therapies to correct the Schwann cell-induced pathology has been demonstrated to be a potent therapeutic strategy for treating CMT1A [15,30,40,41]. The pan PDE4 inhibitor rolipram has previously been demonstrated to enhance myelination *in vivo* when administered simultaneously with transplanting Schwann cells following spinal cord injury [42,43]. Moreover, rolipram promoted oligodendrocyte differentiation and, subsequently, *in vivo* remyelination in an animal model for multiple sclerosis [44]. Specifically in Schwann cells, the PDE4 inhibitor roflumilast was shown to stimulate Schwann cell differentiation, and roflumilast-treated Schwann cells additionally enhanced human iPSC-derived nociceptive axonal outgrowth and myelination [26]. Unfortunately, pan PDE4 inhibition coincides with dose-limiting emetic adverse events hampering its clinical translation. Recently, the PDE4D subtype-specific inhibitor Gebr32a has been demonstrated to enhance CNS neuron outgrowth, remyelination, and oligodendrocyte differentiation, similar to pan PDE4 inhibition without preclinical indications of emetic side effects [28]. Therefore, we investigated in this study whether the PDE4D inhibitor Gebr32a could be considered a valuable treatment strategy for correcting Schwann cell development in a C3-PMP22 mouse model for CMT1A and in CMT1A patient-derived human Schwann cells.

To evaluate the therapeutic potential of the PDE4D inhibitor Gebr32a, we implemented several phenotypical motor function outcomes. We observed a disease-induced phenotype in C3-PMP22 mice as demonstrated by their impaired grip strength, muscle function, motor endurance on the rotarod, and motor coordination on the grid and beam walk when compared to WT animals. Importantly, these motor function outcomes could be significantly improved in C3-PMP22 mice upon PDE4D inhibition. Indeed, Gebr32a-mediated PDE4D inhibition significantly increased grip strength, motor coordination, and evoked motor endurance. We could not observe a clear Gebr32a-mediated PDE4D inhibition effect in the pellet retrieval task. While this task allows the evaluation of fine motor movements in the forelimbs, it has also been demonstrated to highly rely on a motor-skill learning paradigm [20]. Therefore, in contrast to non-learnable evoked motor behavior (e.g., hanging wire and grid walk), the pellet retrieval task not only evaluates motor behavior but rather evaluates the complex motor learning potential of the animals. The difference in the underlying functional and anatomical structures involved potentially explains the lack of efficacy of Gebr32a to improve pellet retrieval success rates.

Importantly, we chose to use two animal cohorts within our study, differing in age and representing both sexes, which gives a good representation of the CMT1A patient population [1,45]. These animals were simultaneously treated and evaluated for functional outcome, and even though both cohorts differed 10–15 weeks of age when Gebr32a treatment was initiated, both responded similarly to the pharmacological treatment. Furthermore, the improved motor functions were accompanied by a reduced latency time of sciatic nerve-stimulated CMAP measures, indicating an increased nerve conduction speed [33]. Due to the high supramaximal intensities required for measuring CMAPs in demyelinating neuropathies (up to 60 mA) [33,46] compared to the supramaximal intensities used in WT animals (5–20 mA), we can conclude that PDE4D inhibition did not completely normalized sciatic nerve signal transduction. Nevertheless, the improved nerve conduction correlates with the enhanced motor functions, implicating that PDE4D inhibition can be considered as a powerful treatment strategy for improving CMT1A disease phenotype [33,46].

Post-mortem analysis of the sciatic nerve revealed that PDE4D inhibition by Gebr32a was accompanied by an enhanced myelination in C3-PMP22 animals as higher levels of the myelin proteins MBP and MPZ, and the Schwann cell differentiation marker KROX20 were observed. Additionally, besides increased myelination, βIII-tubulin protein levels were found to be increased in the sciatic nerve of C3-PMP22 animals upon PDE4D inhibition. βIII-tubulin is a protein member specifically localized to neurons [47], and due to its correlation with neuronal differentiation, it has been implied to be crucially involved in peripheral axon regeneration [47–49]. However, the observed increase in βIII-tubulin in the sciatic nerve of C3-PMP22 animals was somewhat unexpected as no differences were observed in the amplitude of the electrophysiological measurements. Nevertheless, previous research of our research group has already demonstrated that PDE4D inhibition enhances neurite outgrowth *in vitro* [50]. The plasticity-enhancing properties of Gebr32a might, therefore, explain the increase in βIII-tubulin on a molecular level. *Post-mortem* electron microscopy analysis confirmed increased myelination and myelin integrity upon PDE4D inhibition in C3-PMP22 mice, as demonstrated by significantly lower *g*-ratio values and a trend towards an increased myelin sheath thickness. The pathology in nerves of C3-PMP22 mice is quite heterogenous, and not all axons are equally affected. Therefore, we believe by having measured every axon, including healthy ones, that we even have an underestimation of the therapeutic effect of Gebr32a. Although previous studies demonstrated that PDE4D inhibition stimulates neuroplasticity and neurite outgrowth, no significant changes were found on the axon caliber, confirming the CMAP amplitude data [17,18,51]. As a next step, we explored the effect of Gebr32a-mediated PDE4D inhibition on primary mouse Schwann cells isolated from nerves of C3-PMP22 mice. We found that Gebr32a dose-dependently reduced the expression of *c-Jun,* alongside an increase in the expression of the pro-myelinating genes *Oct6*, *Krox20*, *Mbp*, *Mpz*, and *Plp*. These findings indicate a positive effect of the PDE4D inhibitor on Schwann cell differentiation in CMT1A. Unexpectedly, the expression of *c-Jun* and *p75*, a marker of undifferentiated Schwann cells, were not in the same direction. Although p75 and c-Jun serve as markers for early and dedifferentiated Schwann cells, respectively, they operate through independent regulatory mechanisms without a direct link [52]. Furthermore, *p75* expression is influenced by various contextual factors, including signaling pathways, injury states, and the cellular environment. *P75* also significantly affects migration and axon growth during development. When using primary cells in culture, these cells are removed from their *in vivo* context and may exhibit more developmentally oriented behavior, which could partly explain the observed divergence in p75 expression compared to c-Jun. Additionally, it is important to note that qPCR provides a snapshot of mRNA levels at a specific time point, which does not necessarily correlate directly with protein-level changes or functional outcomes.

Similar to the primary mouse Schwann cell data, in iPSC-derived Schwann cells from a CMT1A patient, we observed a reduction in *c-JUN* expression and, moreover, an increased expression of several pro-myelinating genes, including *KROX20, MPZ,* and *MBP,* following Gebr32a treatment. This highlights the clinical translational relevance of our findings. Unexpectedly, *PMP22* expression was downregulated after Gebr32a treatment in both murine and human Schwann cells. Controlling *PMP22* expression by cAMP has been demonstrated by several authors before, strongly suggesting that the absence of cAMP acts as a silencer of *PMP22* expression [53,54]. This observation adds another complex layer to our understanding of PDE4D inhibition in CMT1A.

Although the exact underlying molecular mechanisms remain to be elucidated, downstream key players within the cAMP signaling cascade have been described to be directly involved in the normal function of Schwann cells. In fact, Schwann cell differentiation mainly relies on exchange protein directly activated by cAMP (EPAC) effector proteins, while the mitogenic activity rather involves protein kinase A (PKA) activation [26]. Additionally, both PKA and EPAC effector proteins were observed to directly increase the *Krox20* to *c-Jun* ratio in Schwann cells *in vitro*, thereby driving their differentiation and subsequent myelination, further supporting the role of modulating cAMP signaling to restore Schwann cell defects in CMT1A [17,18,51]. In line, we have previously demonstrated that both dibutyryl-cAMP and a PDE4 inhibitor roflumilast are effective in boosting the expression of myelin genes (MBP, PLP, and MAG) as well as genes related to neurotrophic factors (BDNF, NGF, and GDNF) in primary rat Schwann cells. Interestingly, when

downstream EPAC was inhibited, the expression of myelin genes was hindered after PDE4 inhibition, while PKA inhibition significantly impeded the expression of neurotrophic factor genes. This highlights that EPAC signaling predominantly supports myelination, whereas PKA signaling is more critical for the regulation of neurotrophic factors [26]. However, unfortunately, PDE4 inhibition cannot be therapeutically translated due to the severe emetic side effects accompanied by its administration. Due to the lack of emetic side effects when administering Geb32a, we demonstrate here for the first time the relevance of targeting PDE4D for therapeutic intervention in CMT [28]. Moreover, cyclic nucleotides, such as cGMP and cAMP, are known to control many additional cellular processes. VerPlank *et al.* have demonstrated that cGMP activates the 26S proteasome via protein kinase G (PKG), thereby enhancing protein degradation [55–57]. Specifically, they found that raising cGMP levels restores proteasome function and myelination in mice with proteotoxic neuropathy [58]. Importantly, cAMP has similar effects on the 26S proteasome by Rpn6/PSMD11 phosphorylation [59, 60], and it is, therefore, reasonable to assume that increasing cAMP via PDE4D inhibition may improve the proteasome function in CMT1A models, apart from directly driving Schwann cell differentiation programs.

Taken together, our data demonstrate for the first time that pharmacological PDE4D inhibition by Gebr32a improves functional and molecular aspects of CMT1A pathology, as observed in C3-PMP22 mice, primary murine Schwann cells and CMT1A patient iPSC-derived Schwann cells. These findings underscore the therapeutic potential of PDE4D inhibition in correcting Schwann cell dysfunction in CMT1A, offering promising prospects for disease management.

Ethics approval and consent to participate

The human iPSC line was obtained from a CMT1A patient with consent.

Funding

This work was supported by the Fonds voor Wetenschappelijk Onderzoek (FWO-Vlaanderen). MS is supported by the FWO-Vlaanderen aspirant strategic research (fundamental research postdoc program (project number: 1S57519N, 1S57521N and 1272324N). TV was supported by the FWO-Vlaanderen fundamental research postdoc program, project number 12Z2620N, and UHasselt BOF, project number R-14084. KL was supported by the FWO-Vlaanderen, fundamental aspirant (project number: 11A4120N and 11A4122N). HJ was supported by the FWO-Vlaanderen fundamental research (project number: 11M0222N and 11M0224N). RP was a Strategic Basic (SB) Ph.D. fellow at the FWO-Vlaanderen, project number 1S59317N. RP was also supported by the National University of Ireland, Travelling Studentship. LVDB is supported by VIB, the KU Leuven (C14/22/132 and IDN/22/012), the Association Française les Myopathies (AFM) and the Generet Award for Rare Diseases. LVDB and EW are supported by the VLIR (iBOF/23/021C).

CRediT authorship contribution statement

Hanne Jeurissen: Writing – review & editing, Investigation, Formal analysis. **Esther Wolfs:** Writing – review & editing, Supervision, Conceptualization. **Darren Jacobs:** Writing – review & editing, Methodology, Investigation. **Tim Vanmierlo:** Writing – review & editing, Supervision, Conceptualization. **Elisabeth Piccart:** Writing – review & editing, Methodology, Conceptualization. **Robert Prior:** Writing – review & editing, Methodology, Investigation. **Olga Bruno:** Writing – review & editing, Resources, Methodology. **Melissa Schepers:** Writing – review & editing, Writing – original draft, Methodology, Investigation, Conceptualization. **Jos Prickaerts:** Writing – review & editing, Resources, Methodology. **Tim Vangansewinkel:** Writing – review & editing, Writing – original draft, Project administration, Methodology, Investigation, Conceptualization. **Ivo Lambrichts:** Writing – review & editing, Methodology. **Karen Libberecht:** Writing – review & editing, Writing – original draft, Methodology, Investigation, Conceptualization. **Ludo Van Den Bosch:** Writing – review & editing, Methodology. **Ernesto Fedele:** Writing – review & editing, Resources, Methodology. **Roberta Ricciarelli:** Writing – review & editing, Resources, Methodology. **Chiara Brullo:** Writing – review & editing, Resources, Methodology.

Declaration of Competing Interest

MS, EP, JP and TV have a proprietary interest in selective PDE4D inhibitors for the treatment of demyelinating disorders and neurodegenerative disorders. EW is part of the Scientific Advisory Board of Innoser (Diepenbeek, Belgium). LVDB is head of the Scientific Advisory Board of Augustine Therapeutics (Leuven, Belgium) and is part of the Investment Advisory Board of Droia Ventures (Meise, Belgium). The other authors declare no competing interests.

Acknowledgements

The authors would like to thank Marc Jans and Wendy Vandendries for their help with the processing and analysis of the transmission electron microscopy images. We would also like to thank Cedars-Sinai and Dr. Robert H. Baloh for the development of the CMT1A iPSC line used in this study.

Author contributions

MS, TV, and KL conceptualized and designed the study, with input from TVM and EW. TV, KL and MS performed the subcutaneous injections on the animals and did the *in vivo* follow-ups. TV, DJ and MS performed and analyzed the functional assays. TV, DJ and EP performed the *in vivo* electrophysiological recordings and motor phenotyping. RP developed the iPSC-SC protocol and provided help with the electrophysiological measurements *in vivo*. HJ and KL performed the primary mouse Schwann cell isolations and human cell culture. MS processed the *in vitro* samples and performed the qPCR experiment and analysis. KL, TV, HJ, and MS performed the analysis of the electron microscopic images. KL, HJ, TV, and MS performed histological experiments and analysis on extracted tissues from WT and C3-PMP22 mice. CB and OB designed and synthesized Gebr32a. RR, CB, EF, OB and JP developed the Gebr32a compound and revised the manuscript. IL and LVDB provided insight and critical feedback throughout the project. MS, TV, and KL wrote the manuscript and revised and finalized the manuscript with the help of LVDB, TVM, and EW. All authors participated in finalizing the manuscript.

Consent for publication

All authors have approved the contents of this study and provided consent for publication.

Data Availability

Data will be made available on request. All data from this study are available from the corresponding authors on reasonable request.

References

[1] M. Juneja, et al., Challenges in modelling the Charcot-Marie-Tooth neuropathies for therapy development, J. Neurol. Neurosurg. Psychiatry 90 (1) (2019) 58–67.
[2] B. W. van Paassen, et al., PMP22 related neuropathies: Charcot-Marie-Tooth disease type 1A and hereditary neuropathy with liability to pressure palsies, Orphanet J. Rare Dis. 9 (2014) 38.

[3] R. Prior, et al., Defective axonal transport: a common pathological mechanism in inherited and acquired peripheral neuropathies, Neurobiol. Dis. 105 (2017) 300–320.
[4] V. Benoy, et al., HDAC6 is a therapeutic target in mutant GARS-induced Charcot-Marie-Tooth disease, Brain 141 (3) (2018) 673–687.
[5] K. Szigeti, J.R. Lupski, Charcot-Marie-Tooth disease, Eur. J. Hum. Genet 17 (6) (2009) 703–710.
[6] V. Timmerman, A.V. Strickland, S. Zuchner, Genetics of Charcot-Marie-Tooth (CMT) Disease within the Frame of the Human Genome Project Success, Genes (Basel) 5 (1) (2014) 13–32.
[7] J. Baets, P. De Jonghe, V. Timmerman, Recent advances in Charcot-Marie-Tooth disease, Curr. Opin. Neurol. 27 (5) (2014) 532–540.
[8] V. Timmerman, et al., The peripheral myelin protein gene PMP-22 is contained within the Charcot-Marie-Tooth disease type 1 A duplication, Nature (1992).
[9] M. Pennuto, et al., Ablation of the UPR-mediator CHOP restores motor function and reduces demyelination in Charcot-Marie-Tooth 1B mice, Neuron 57 (3) (2008) 393–405.
[10] B. Gess, et al., Ascorbic acid for the treatment of Charcot-Marie-Tooth disease, Cochrane Database Syst. Rev. 2015 (12) (2015). CD011952.
[11] M.W. Sereda, K.A. Nave, Animal models of Charcot-Marie-Tooth disease type 1A, Neuromol. Med. 8 (1-2) (2006) 205–216.
[12] M. Bush, The role of unconscious guilt in psychopathology and psychotherapy, Bull. Menn. Clin. 53 (2) (1989) 97–107.
[13] M. Grandis, M.E. Shy, Current Therapy for Charcot-Marie-Tooth disease, Curr. Treat. Options Neurol. 7 (1) (2005) 23–31.
[14] P.V. Monje, To myelinate or not to myelinate: fine tuning cAMP signaling in Schwann cells to balance cell proliferation and differentiation, Neural Regen. Res 10 (12) (2015) 1936–1937.
[15] R. Fledrich, et al., Soluble neuregulin-1 modulates disease pathogenesis in rodent models of Charcot-Marie-Tooth disease 1A, Nat. Med 20 (9) (2014) 1055–1061.
[16] A. Kiepura, K. Andrzej, Charcot-Marie-Tooth type 1A drug therapies: role of adenylyl cyclase activity and G-protein coupled receptors in disease pathomechanism, Acta Neurobiol. Exp. 78 (2018) 198–209.
[17] K.R. Jessen, R. Mirsky, L. Morgan, Role of cyclic AMP and proliferation controls in schwann cell differentiation, Ann. N. Y Acad. Sci. 633 (1991).
[18] P.V. Monje, et al., Schwann cell dedifferentiation is independent of mitogenic signaling and uncoupled to proliferation: role of cAMP and JNK in the maintenance of the differentiated state, J. Biol. Chem. 285 (40) (2010) 31024–31036.
[19] J. Li, et al., The PMP22 gene and its related diseases, Mol. Neurobiol. 47 (2) (2013) 673–698.
[20] L. Nobbio, et al., The diadenosine homodinucleotide P18 improves in vitro myelination in experimental Charcot-Marie-Tooth type 1A, J. Cell Biochem 115 (1) (2014) 161–167.
[21] D. Paes, et al., The molecular biology of phosphodiesterase 4 enzymes as pharmacological targets: an interplay of isoforms, conformational states, and inhibitors, Pharm. Rev. 73 (3) (2021) 1016–1049.
[22] M. Schepers, et al., Targeting phosphodiesterases-towards a tailor-made approach in multiple sclerosis treatment, Front. Immunol. 10 (2019) 1727.
[23] A.J. Tibbo, G.S. Tejeda, G.S. Baillie, Understanding PDE4's function in Alzheimer's disease; a target for novel therapeutic approaches, Biochem Soc. Trans. 47 (5) (2019) 1557–1565.
[24] E. Nikulina, et al., The phosphodiesterase inhibitor rolipram delivered after a spinal cord lesion promotes axonal regeneration and functional recovery, PNAS (2004).
[25] E. Udina, et al., Rolipram-induced elevation of cAMP or chondroitinase ABC breakdown of inhibitory proteoglycans in the extracellular matrix promotes peripheral nerve regeneration, Exp. Neurol. 223 (1) (2010) 143–152.
[26] M. Schepers, et al., Phosphodiesterase (PDE) 4 inhibition boosts Schwann cell myelination in a 3D regeneration model, Eur. J. Pharm. Sci. 185 (2023) 106441.
[27] A. Robichaud, et al., Deletion of phosphodiesterase 4D in mice shortens alpha(2)-adrenoceptor-mediated anesthesia, a behavioral correlate of emesis, J. Clin. Invest 110 (7) (2002) 1045–1052.
[28] M. Schepers, et al., Selective PDE4 subtype inhibition provides new opportunities to intervene in neuroinflammatory versus myelin damaging hallmarks of multiple sclerosis, Brain Behav. Immun. 109 (2023) 1–22.
[29] Cea Verhamme, Myelin and axon pathology in a long-term study of PMP22-overexpressing mice, J. Neuropathol. Exp. Neurol. 70 (2011) 386–398.
[30] R. Prior, et al., HDAC3 Inhibition Stimulates Myelination in a CMT1A Mouse Model, Mol. Neurobiol. 59 (6) (2022) 3414–3430.
[31] J. Hantke, et al., c-Jun activation in Schwann cells protects against loss of sensory axons in inherited neuropathy, Brain 137 (Pt 11) (2014) 2922–2937.
[32] R. Ricciarelli, et al., Memory-enhancing effects of GEBR-32a, a new PDE4D inhibitor holding promise for the treatment of Alzheimer's disease, Sci. Rep. 7 (2017) 46320.
[33] E. Pollari, et al., In vivo electrophysiological measurement of compound muscle action potential from the forelimbs in mouse models of motor neuron degeneration, J. Vis. Exp. (136) (2018).
[34] N.D. Andersen, P.V. Monje, Isolation, culture, and cryopreservation of adult rodent schwann cells derived from immediately dissociated teased fibers, Methods Mol. Biol. 1739 (2018) 49–66.
[35] N.D. Andersen, et al., A rapid and versatile method for the isolation, purification and cryogenic storage of Schwann cells from adult rodent nerves, Sci. Rep. 6 (2016) 31781.
[36] M.H. Kim, et al., Conditioned medium from the three-dimensional culture of human umbilical cord perivascular cells accelerate the migration and proliferation of human keratinocyte and fibroblast, J. Biomater. Sci. Polym. Ed. 29 (7-9) (2018) 1066–1080.
[37] Y. Cai, et al., Chloroquine affects autophagy to achieve an anticancer effect in EC109 esophageal carcinoma cells in vitro, Oncol. Lett. 15 (1) (2018) 1143–1148.
[38] H.S. Kim, et al., Schwann cell precursors from human pluripotent stem cells as a potential therapeutic target for myelin repair, Stem Cell Rep. 8 (6) (2017) 1714–1726.
[39] R. Prior, et al., PMP22 duplication dysregulates lipid homeostasis and plasma membrane organization in developing human Schwann cells, Brain (2024).
[40] R. Fledrich, et al., Targeting myelin lipid metabolism as a potential therapeutic strategy in a model of CMT1A neuropathy, Nat. Commun. 9 (1) (2018) 3025.
[41] E. Passage, et al., Ascorbic acid treatment corrects the phenotype of a mouse model of Charcot-Marie-Tooth disease, Nat. Med 10 (4) (2004) 396–401.
[42] D.D. Pearse, et al., cAMP and Schwann cells promote axonal growth and functional recovery after spinal cord injury, Nat. Med. 10 (6) (2004) 610–616.
[43] G. Flora, et al., Combining neurotrophin-transduced schwann cells and rolipram to promote functional recovery from subacute spinal cord injury, Cell Transpl. 22 (12) (2013) 2203–2217.
[44] Y.A. Syed, et al., Inhibition of phosphodiesterase-4 promotes oligodendrocyte precursor cell differentiation and enhances CNS remyelination, EMBO Mol. Med. 5 (12) (2013) 1918–1934.
[45] B.W. van Paassen, et al., PMP22 related neuropathies: Charcot-Marie-Tooth disease type 1A and hereditary neuropathy with liability to pressure palsies, Orphanet J. Rare Dis. 9 (2014) 38.
[46] V. Parker, et al., Supramaximal stimulus intensity as a Diagnostic Tool in Chronic demyelinating neuropathy, Neurosci. J. 2016 (2016) 6796270.
[47] A. Ferreira, A. Caceres, Expression of the class III beta-tubulin isotype in developing neurons, J. Neurosci. Res 32 (1992).
[48] A. Latremoliere, et al., Neuronal-Specific TUBB3 is not required for normal neuronal function but is essential for timely axon regeneration, Cell Rep. 24 (2018).
[49] Y.Q. Jiang, M.M. Oblinger, Differential regulation of beta III and other tubulin genes during peripheral and central neuron development, J. Cell Sci. 103 (1992).
[50] D. Paes, et al., Ablation of specific long PDE4D isoforms increases neurite elongation and conveys protection against amyloid-beta pathology, Cell Mol. Life Sci. 80 (7) (2023) 178.
[51] K. Bacallao, P.V. Monje, Requirement of cAMP signaling for Schwann cell differentiation restricts the onset of myelination, PLoS One 10 (2) (2015) e0116948.
[52] Delara Saberan-Djoneidi, et al., Molecular dissection of the Schwann cell specific promoter of the PMP22 gene, Gene (2000).
[53] Q. Yuan, et al., P75 and phosphorylated c-Jun are differentially regulated in spinal motoneurons following axotomy in rats, Neural Regen. Res 7 (26) (2012) 2005–2011.
[54] F. Kaya, et al., Ascorbic acid inhibits PMP22 expression by reducing cAMP levels, Neuromuscul. Disord. 17 (3) (2007) 248–253.
[55] J.J.S. VerPlank, et al., Impairment of protein degradation and proteasome function in hereditary neuropathies, Glia 66 (2) (2018) 379–395.
[56] Y. Bai, et al., Treatment with IFB-088 improves neuropathy in CMT1A and CMT1B mice, Mol. Neurobiol. 59 (7) (2022) 4159–4178.
[57] J.J.S. VerPlank, et al., cGMP via PKG activates 26S proteasomes and enhances degradation of proteins, including ones that cause neurodegenerative diseases, Proc. Natl. Acad. Sci. USA 117 (25) (2020) 14220–14230.
[58] J.J.S. VerPlank, et al., Raising cGMP restores proteasome function and myelination in mice with a proteotoxic neuropathy, Brain 145 (1) (2022) 168–178.
[59] J.J.S. VerPlank, et al., 26S Proteasomes are rapidly activated by diverse hormones and physiological states that raise cAMP and cause Rpn6 phosphorylation, Proc. Natl. Acad. Sci. USA 116 (10) (2019) 4228–4237.
[60] S. Lokireddy, N.V. Kukushkin, A.L. Goldberg, cAMP-induced phosphorylation of 26S proteasomes on Rpn6/PSMD11 enhances their activity and the degradation of misfolded proteins, Proc. Natl. Acad. Sci. USA 112 (52) (2015). E7176-85.